Heat transfer in the thermally developing region of a pulsating channel flow

SEO YOUNG KIM,† BYUNG HA KANG‡ and JAE MIN HYUN†§

†Department of Mechanical Engineering, Korea Advanced Institute of Science and Technology,
Yusungku, Taejon, 305-701, Korea
‡Thermal/Fluids Engineering Laboratory, Korea Institute of Science and Technology, Seoul, Korea

Abstract—A study is made of the heat transfer characteristics of a fully-developed pulsating flow in a channel. The fluid at the channel inlet is of temperature T_o, and the channel walls are at uniform temperature T_w. Concern is directed to the thermally developing region. The unsteady Navier–Stokes equations are solved numerically to simulate a relatively slow throughflow at $Re = 50$, $Pr = 0.7$. Comprehensive time-dependent flow data are obtained for wide ranges of two key parameters, i.e. the pulsation amplitude $0 \leq A \leq 0.75$, and the nondimensional pulsation frequency M up to 10.0. When M is low, the velocity profiles resemble much of the quasi-steady solutions. When M is large, the effects of oscillation are confined to a narrow zone adjacent to the walls. The changes in the Nusselt number Nu due to pulsation are pronounced in the entrance region, say $X/(Re \cdot Pr) < 1.0$, and the impact of pulsation on Nu is minor at far downstream locations. The effects of M on Nu are noticeable when M is small and moderate. At high pulsation frequencies, heat transfer is little affected by the addition of pulsation. Detailed analyses on local behavior of heat transfer are made by using Fourier-series representations of the numerical results. These exercises indicate that, due to pulsation, both heat transfer enhancement and reduction can be expected in various axial locations of the channel. Based on these numerical results, physically plausible explanations are offered to interpret the axial behavior of heat transfer.

1. INTRODUCTION

THE CHARACTERISTICS of a pulsating flow in a confined passageway have received considerable attention in recent years. The classical analyses [1, 2] identified the pertinent nondimensional parameters: the Reynolds number of the average flow, and the dimensionless amplitude and frequency of pulsation. When the pulsation amplitude is small, the theoretical endeavors, under several restrictive assumptions, clarified the velocity distribution and phase relationship of the pulsating flow in a duct or a pipe. These rudimentary findings were found to be in general agreement with some of the available experimental measurements over limited ranges [3–8].

Studies of the attendant heat transfer characteristics of a pulsating flow in a duct have been far less numerous, and the existing investigations have often offered conflicting results [9–15]. The obvious main question is how heat transfer is influenced by the presence of pulsation. This poses an issue of fundamental importance from the standpoint of basic research of unsteady convective heat transfer processes. Also, in practical applications, concern has been directed to the feasibility of enhancing heat transport by adding pulsation components to the throughflow in a duct. As observed by Hwang and Dybbs [9] and Simon and Seume [10], however, experimental data on this topic are meager and incomplete.

The physical phenomena underlying the unsteady

convective heat transfer are rather complex. Consequently, in an effort to acquire a proper understanding of the physical process, several models, which contain greatly simplified approximations, have been proposed. Despite their simplicity, these models have been presumed to depict the central elements of the physical systems under study.

It is notable that the accounts by Siegel and Perlmutter [11] and Faghri *et al.* [12], by resorting to theoretical idealized models, explored the principal character of heat transfer of a pulsating flow in a pipe (or a channel). In particular, Siegel and Perlmutter [11] demonstrated the explicit dependence of the overall heat transfer on pulsation frequency. Furthermore, when a constant-temperature wall boundary condition was adopted, the resulting Nusselt number showed a periodic axial variation. These analytical undertakings pointed out the significance of the interaction between the velocity and temperature oscillations, which could lead to increased heat transfer rates.

The above-stated theoretical models laid the groundwork to ascertain the eminent physical processes at work in convective heat transfer of a pulsating flow in a duct. However, it is equally important to inquire as to the applicability of the simplifications of these models to more realistic situations. First of all, the analyses of refs. [11, 12] were based on strictly linearized, one-dimensional-like approximations. The resulting velocity and temperature fields were considered to be the algebraic combination of a non-pulsating part and a sinusoidally varying oscillating part. These approximations were necessary to carry

§Author to whom all correspondence should be addressed.

NOMENCLATURE

A	oscillating amplitude of axial velocity	X, Y	dimensionless axial and transverse coordinates
B	axial pressure gradient, $-(\partial P/\partial X)$		
C_f	skin friction coefficient, $\sigma_w/(1/2\rho U_0^2)$	X^*	inverse of the Graetz number, $X/(Re\ Pr)$.
C_p	specific heat of fluid		
F	axial additional convective term		
G_0, G_n	time-dependent fluctuation of axial temperature gradient	**Greek symbols**	
		α	thermal diffusivity, $k/\rho C_p$
H	half-width of flow channel	θ	dimensionless temperature
k	thermal conductivity	θ'	fluctuating part of dimensionless temperature
$L1$	length of unheated section		
$L2$	length of heated section	θ_b	dimensionless bulk temperature
M	frequency parameter, $H(\omega/2v)^{1/2}$	μ	dynamic viscosity
Nu	Nusselt number, $d\theta/dY\vert_{Y=1}$	v	kinematic viscosity
P	pressure	ρ	density
Pe	Peclet number, $Re\ Pr$	τ	dimensional time
Pr	Prandtl number, v/α	ϕ	phase.
Re	Reynolds number, $U_0 H/v$		
t	dimensionless time	**Subscripts**	
T	dimensional temperature	1	primary oscillating component
T'	fluctuating part of temperature	m	time mean value
u, v	dimensional velocity components	n	harmonics index
U, V	dimensionless velocity components	o	reference values
u'	fluctuating part of velocity	s	non-pulsating component
x, y	dimensional axial and transverse coodinates	t	time-dependent component
		w	wall.

out analytical treatments of extremely complicated physical systems. In addition, in the treatise of ref. [11], the fluid velocity was taken to be fully developed. Furthermore, when the simplified energy equation was solved, the slug flow assumption was introduced. In the case of the theoretical examinations by Faghri *et al.* [12], similar linearized formulations were invoked. Also, Faghri *et al.* confined their linearized analyses to the parameter ranges of asymptotically low values of the pulsation frequency parameter.

As emphasized previously, Faghri *et al.* [12] clearly brought into focus the major physical mechanisms at work, which stem from the interactions between the temperature and velocity oscillations. The results of these highly idealized analytical efforts yielded an improved understanding of the principal structures of unsteady flow and thermal fields. It has also to be stressed, however, that the underlying assumptions and approximations embedded in these theoretical models have not been critically assessed. As mentioned earlier, experimental measurements have been scanty and sketchy; consequently, the scope and limitations of these preceding theoretical accounts have not been appraised by other independent means. One alternative route is to conduct full-dress numerical simulations of pulsating flow and heat transfer properties, and these issues are now addressed in this paper. The main objective is to encompass the parameter spaces that were difficult to cover by the previous theoretical means.

In the present work, numerical solutions to the unsteady, two-dimensional, elliptic-type Navier–Stokes equations for a pulsating flow in a channel will be sought. The purpose is to secure comprehensive numerical solutions for the flow configuration of Siegel and Perlmutter [11] over broad ranges of the key nondimensional parameters. The outcome of these extensive numerical exercises provides the details of unsteady flow and thermal fields. The numerical results allow reevaluations of the suitability of the simplifying assumptions and approximations which were incorporated in the above theoretical models.

It is noteworthy that some of the earlier numerical attempts [14] utilized the boundary-layer equations. However, if the pulsation amplitude is large, there arises the possibility of significant flow reversals near the wall; this would cast doubt on the usefulness of the parabolic-type boundary-layer-flow treatments. The present formulation of full Navier–Stokes equations can overcome these difficulties, and, henceforth, it is selected in this study.

2. FORMULATION

The channel flow geometry, coordinates (x, y) and velocity components (u, v) are shown in Fig. 1. This is in accordance with the problem statement of ref. [11]. The pulsating flow of constant temperature T_0 at the inlet is given in the form of
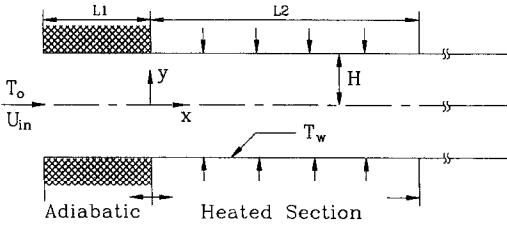
FIG. 1. Schema of the flow configuration.

$$U_{in} = U_o(1 + A \sin \omega\tau). \tag{1}$$

As remarked in ref. [11], an unheated hydrodynamic entrance region of length $L1$ exists at the inlet, which is followed by a heated region of length $L2$. On the channel wall of $L2$, the condition of constant surface temperature T_w is imposed.

The full, time-dependent, incompressible Navier–Stokes equations, in properly nondimensionalized form, can be written, using standard notation, as

$$\frac{\partial U}{\partial X} + \frac{\partial V}{\partial Y} = 0 \tag{2}$$

$$\frac{\partial U}{\partial t} + U\frac{\partial U}{\partial X} + V\frac{\partial U}{\partial Y} = -\frac{\partial P}{\partial X} + \frac{1}{Re}\left(\frac{\partial^2 U}{\partial X^2} + \frac{\partial^2 U}{\partial Y^2}\right) \tag{3}$$

$$\frac{\partial V}{\partial t} + U\frac{\partial V}{\partial X} + V\frac{\partial V}{\partial Y} = -\frac{\partial P}{\partial Y} + \frac{1}{Re}\left(\frac{\partial^2 V}{\partial X^2} + \frac{\partial^2 V}{\partial Y^2}\right) \tag{4}$$

$$\frac{\partial \theta}{\partial t} + U\frac{\partial \theta}{\partial X} + V\frac{\partial \theta}{\partial Y} = \frac{1}{Pe}\left(\frac{\partial^2 \theta}{\partial X^2} + \frac{\partial^2 \theta}{\partial Y^2}\right). \tag{5}$$

In the above, the nondimensional quantities are defined as

$$U \equiv \frac{u}{U_o}, \quad V \equiv \frac{v}{U_o}, \quad X \equiv \frac{x}{H}, \quad Y \equiv \frac{y}{H},$$

$$t \equiv \frac{\tau}{H/U_o}, \quad P \equiv \frac{p}{\rho U_o^2}, \quad Re = U_o H/v, \quad Pr = v/\alpha,$$

$$Pe = Re\, Pr = U_o H/\alpha, \quad \theta \equiv \frac{T - T_o}{T_w - T_o} \tag{6}$$

where, v is the kinematic viscosity, α the thermal diffusivity.

The associated boundary conditions are now considered. At the channel inlet, a unidirectional, pulsating flow of uniform temperature is assumed, as described above:

at $X = -L1$, for $0 < Y < 1$,

$$U(-L1, Y, t) = 1 + A \sin\left(\frac{2M^2}{Re}t\right) \tag{7a}$$

$$V(-L1, Y, t) = 0 \tag{7b}$$

$$\theta(-L1, Y, t) = 0. \tag{7c}$$

In (7a), the nondimensional pulsation frequency

parameter, $M = H(\omega/2v)^{1/2}$, emerges at the inlet flow conditions.

At the channel walls,

at $Y = 1$, for $-L1 < X < 0$

$$U(X, 1, t) = 0 \tag{7d}$$

$$V(X, 1, t) = 0 \tag{7e}$$

$$\frac{\partial \theta}{\partial Y}(X, 1, t) = 0 \tag{7f}$$

at $Y = 1$, for $0 < X < L2$

$$U(X, 1, t) = 0 \tag{7g}$$

$$V(X, 1, t) = 0 \tag{7h}$$

$$\theta(X, 1, t) = 1. \tag{7i}$$

Owing to the symmetry requirement at the channel centerline, we have

at $Y = 0$, for $-L1 < X < L2$

$$\frac{\partial U}{\partial Y}(X, 0, t) = 0 \tag{7j}$$

$$V(X, 0, t) = 0 \tag{7k}$$

$$\frac{\partial \theta}{\partial Y}(X, 0, t) = 0. \tag{7l}$$

At the channel exit, the flow is assumed to have attained a fully developed state. This is the usual procedure (see [4, 5]) when a long channel is considered, i.e. $L2 \gg 1$. It is worth pointing out that this assumption of negligible gradients of velocity and temperature at the outlet ($X = L2$) becomes more compatible if the outlet is connected to a long channel. Figure 1 illustrates this condition. Accordingly, at $X = L2$, for $0 < Y < 1$

$$\frac{\partial U}{\partial X}(L2, Y, t) = 0 \tag{7m}$$

$$\frac{\partial V}{\partial X}(L2, Y, t) = 0 \tag{7n}$$

$$\frac{\partial \theta}{\partial X}(L2, Y, t) = 0. \tag{7o}$$

In order to solve the above system of equations, the well established numerical solution technique, SIMPLER algorithm of Patanker [16], was employed. In the present computations, typically 30–1500 iterations were required for the local variables to achieve convergence. For convergence criteria, the relative variations of axial velocity and of temperature between two successive iterations were smaller than the preassigned accuracy levels of 10^{-4}. In actual calculations, the well-known steady non-pulsating flow was used as the initial-state conditions. In most cases, temporally periodic solutions were obtained after 2–8 cycles of pulsation oscillation. The time resolution was such that one pulsating period was divided by 120 time steps. The spatial mesh points were typically

120 × 25 in the *X–Y* computational domain. The sensitivity of the calculated results to the grid interval, time step and accuracy level in the convergence criteria was checked by repeating calculations. The computational parameters that were selected in the present work were found to yield satisfactory results in the grid- and time step-convergence tests.

3. RESULTS AND DISCUSSIONS

In the actual implementations of numerical calculations, it was chosen that *L*1 = 100.0, *L*2 = 210.0 to simulate a long channel. After several sample computations, these values were found [11–15] to produce developed flows in the heated portion of the channel as well as satisfy, to a fair degree of accuracy, the imposed exit boundary conditions. In accordance with the basic laminar flow formulations of refs. [11–15], the Reynolds and Prandtl numbers were set respectively at *Re* = 50.0, *Pr* = 0.7. This low value of *Re* is selected to simulate a reasonably slow throughflow. As observed by Siegel [11, 13], the impact of pulsation is more clearly seen for slow flows.

The pulsation amplitude was varied $0 \leqslant A \leqslant 0.75$. These relatively large values of *A* were intended to examine the situations in which significant nonlinear pulsation effects are present. Another crucial element of this study is to encompass wide ranges of the pulsation frequency parameter *M*. In the present numerical efforts, *M* varied up to 10.0.

First, the velocity field data are recapitulated. In Fig. 2, the normalized time-dependent part of the fully developed velocity, U_{t-s}, is plotted, and comparisons are made with the results of the essentially one-dimensional analysis of ref. [11]. When *M* is low, as illustrated in Fig. 2(a), the velocitiy profiles resemble much of the quasi-state solutions, i.e. at each time instant, the velocity field is substantially similar to that of a non-pulsating flow driven by the instantaneous axial

pressure gradient. On the other hand, when *M* is large (see Fig. 2(b)), the time-dependent velocity component U_{t-s} is very small in magnitude (note the difference in scales used for the ordinates of Figs. 2(a) and (b)). Furthermore, the *Y*-profiles of U_{t-s} are fairly flat in much of the channel interior, but U_{t-s} varies rapidly in the areas close to the channel wall. This is consistent with the physical interpretations that, when *M* is large, the effects of oscillation tend to be confined to a narrow zone adjacent to the walls [14]. As demonstrated in Fig. 2, the present numerical solutions are in satisfactory overall agreement with the predictions of the previous theoretical models.

The temporal behavior of axial pressure gradient (*B*) and of skin friction coefficient (*C_f*) in the fully-developed region is plotted in Fig. 3. When *M* is low, both the axial pressure gradient and skin friction are nearly in phase with the inlet velocity. However, when *M* is large, the pulsation effects are noticeable. The magnitudes of the oscillating components are substantial. Also, the phase leads, over the inlet velocity, of the axial pressure gradient and of skin friction approach 90° and 45°, respectively. These findings serve to reconfirm the qualitative correctness of the well-documented preceding analytical predictions [1, 2] on the flow properties.

The main topic of the heat transfer characteristics will be dealt with. The physical variable Nu_{t-s} represents the difference between the Nusselt number for the pulsating flow and that for the non-pulsating flow (*A* = 0) under otherwise similar conditions. The axial locations are plotted by using the inverse of the Graetz number, $X^* = X/(Re \cdot Pr)$ (see ref. [11]).

Figure 4(a) exemplifies the axial profile of Nu_{t-s} when *A* is reasonably small. It is obvious that, at downstream axial locations $X/(Re \cdot Pr) > 1.5$, the influence of pulsation is quite minor. The changes in *Nu* due to the pulsation are pronounced in the regions of small $X/(Re \cdot Pr)$ of the heated channel. The sim-
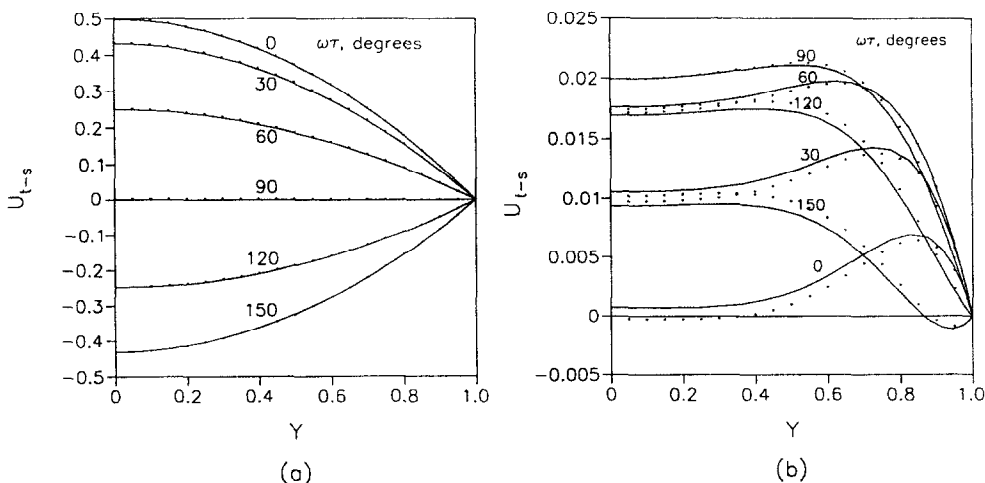
FIG. 2. *Y*-profiles of the time-dependent fluctuation of *u* velocity. ——, the present calculations; · · ·, analytic solutions [11]. The frequency parameters are: (a) *M* = 0.1; (b) *M* = 5.0.
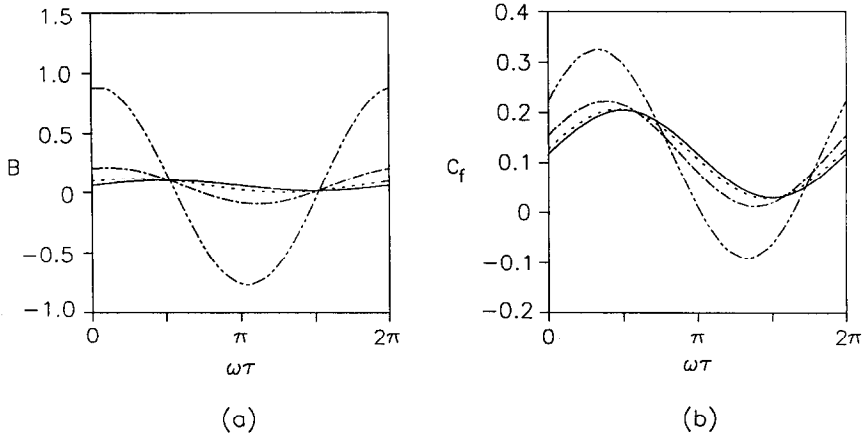
FIG. 3. Time variations of (a) axial pressure gradient, B, and (b) skin friction coefficient, C_f. $A = 0.75$.
———, $M = 0.1$; — — —, $M = 1.0$; —·—, $M = 2.0$; —··—, $M = 5.0$.

plified analytical predictions of Siegel and Perlmutter are in broad qualitative consistency with the present numerical results. When A is appreciable, Fig. 4(b) indicates substantial effects of pulsation in small-X^* regions, say $X^* < 1.0$. The quantitative discrepancy between the analytical results of ref. [11] and the present numerical data is seen as A increases. An inspection of Fig. 4, as well as the spectrum analyses of these plots, is quite revealing. When the pulsation amplitude A is small, as shown in Fig. 4(a), the temporal behavior of Nu_{t-s} is fairly symmetric about the half-period point. When A is appreciable, the profiles of Nu_{t-s} are increasingly non-symmetric about the half-period point. Clearly, Nu_{t-s} is periodic with the imposed pulsation period 2π; however, the presence of the higher harmonics, with shorter periods, is discernible in Fig. 4(b). It is worth pointing out that the power spectrum of the velocity field itself does not contain notable contributions of the higher harmonics

[1, 2, 11, 14]. The heat transport, on the other hand, appears to be significantly affected by the presence of the higher harmonics. As will be asserted later, the nonlinear coupling of velocity and temperature oscillations leads to considerable contributions to heat transfer, and this is reflected in the Nu_{t-s} plots of Fig. 4(b).

The impacts of other relevant parameters on heat transfer are delineated. Figure 5 shows the effect of M on $(Nu_{t-s})_m$, the time-averaged Nu_{t-s}. For low and moderate frequencies, say M up to approximately 1.0, the changes in heat transfer due to pulsation are appreciable throughout much of the channel length. At high frequencies, $M > 1.0$, relatively small changes in heat transfer are visible in and near the entrance regions $X/(Re \cdot Pr) < 1.0$; in the bulk of downstream regions of the channel, heat transfer remains virtually unchanged by the addition of pulsation. The effect of A is exemplified in Fig. 6. As anticipated, changes in
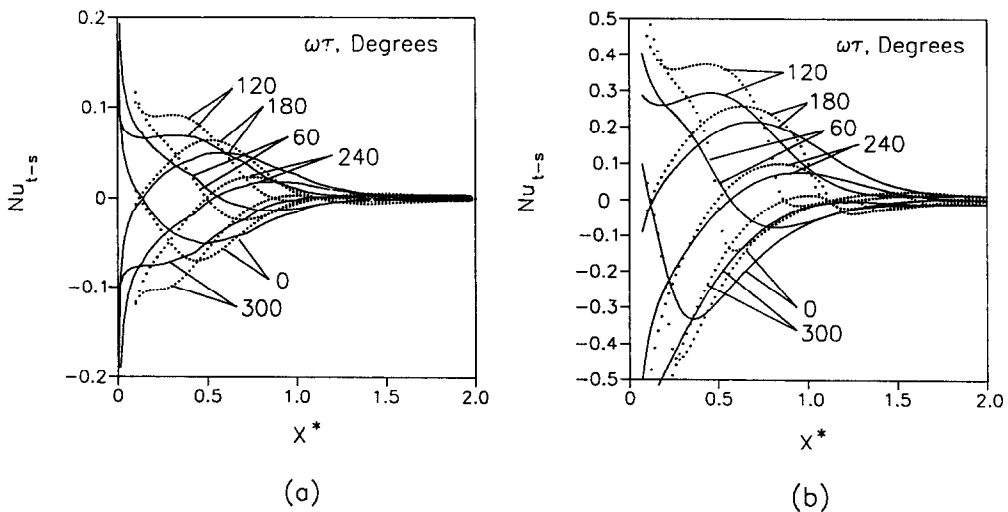
FIG. 4. Axial behavior of Nu_{t-s} at various times. Nu_{t-s} denotes the difference between Nu for a pulsating flow and Nu for a non-pulsating flow under otherwise similar conditions. $M = 2.0$. ———, the present calculations; ···, analytic solutions [11]. (a) $A = 0.15$; (b) $A = 0.75$.
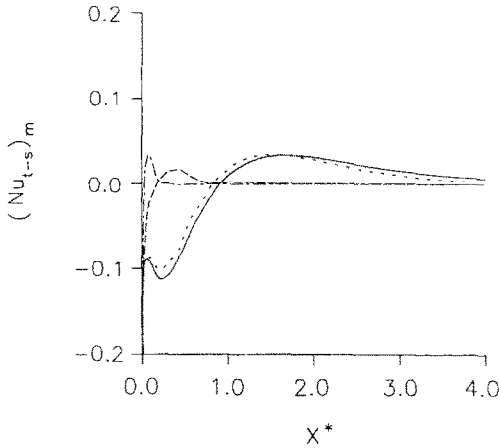
FIG. 5. Time averaged values of Nu_{t-s}. $A = 0.75$.
——, $M = 0.1$; - - -, $M = 1.0$; — — —, $M = 3.0$; —·—·—,
$M = 5.0$.
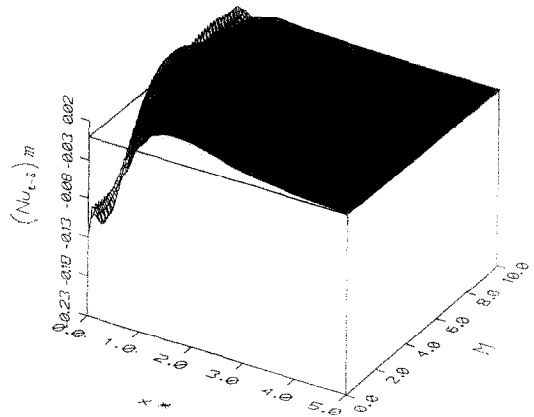
FIG. 7. Plots of $[Nu_{t-s}]_m$ as a function of X^* and M. $A = 0.75$.

heat transfer are enlarged as A increases, especially in the upstream regions near the entrance.

Compiling the comprehensive numerical results, the axial behavior of $(Nu_{t-s})_m$ is displayed as functions of M in Fig. 7. This picture identifies the respective regimes in which the basic character of heat transfer shows qualitative changes. As ascertained previously, the influence of pulsation is notable in the upstream regions of the heated channel, and this is more pronounced at low frequencies. These trends are portrayed in Fig. 8, which illustrates the characteristic regimes in the projected $M-X^*$ plane. Zone (I) denotes negative $(Nu_{t-s})_m$; this implies that, at low frequencies and in the extreme upstream region close to the entrance region, the effect of pulsation tends to reduce heat transfer. Zone (II) represents positive $(Nu_{t-s})_m$; this indicates that, at low frequencies and in moderate downstream axial locations, heat transfer is enhanced owing to the pulsation. The net changes in Nu are rather meager in zone (III) and, therefore, they are of less interest (e.g. $|(Nu_{t-s})_m| < 10^{-2}$). Another finding is that the shape of the demarcation

line, which divides zones (I) and (II), is determined principally by M and far less by A. The pulsation amplitude A has strong influence on the quantitative value of $(Nu_{t-s})_m$ (see Fig. 6); however, the overall qualitative characteristic patterns of $(Nu_{t-s})_m$ in the $M-X^*$ plane are little affected by A.

Summarizing the numerical results exhibited in Figs. 5–8, it is obvious that the effect of pulsation either enhances or reduces the local heat transfer, depending primarily on the axial locations concerned and on the frequency parameter. The physical mechanism underlying this selective behavior of local heat transfer enhancement or reduction is explored. For this purpose, the prior analysis by Faghri et al. [12] provides guidance. It was pointed out in ref. [12] that the axial advective terms of the energy equation play a major role in the determination of the overall heat transports in a pulsating flow. Following the procedures utilized in Faghri et al. [12], the magnitude of each term in the time-averaged energy equation for a pulsating flow was plotted for detailed comparison with that for a non-pulsating flow ($A = 0$). The outcome of this laborious exercise discloses that the
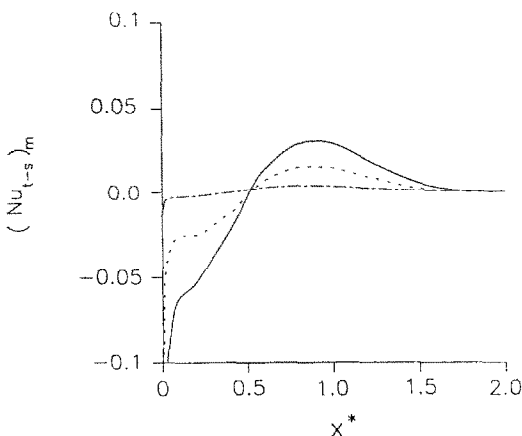
FIG. 6. Time averaged values of Nu_{t-s}. $M = 2.0$. ——,
$A = 0.75$; · · ·, $A = 0.50$; —·—·, $A = 0.15$.
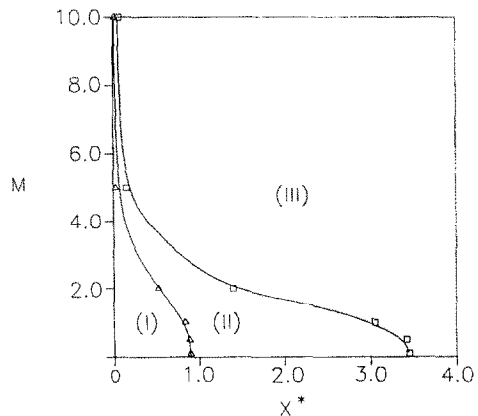
FIG. 8. Exemplary plots of $[Nu_{t-s}]_m$ on the $M-X^*$ plane. Zones (I), (II) and (III) denote reductions, enhancements and no-changes (i.e. $[Nu_{t-s}]_m < 10^{-2}$) of local heat transfer over the non-pulsating flow values, respectively.
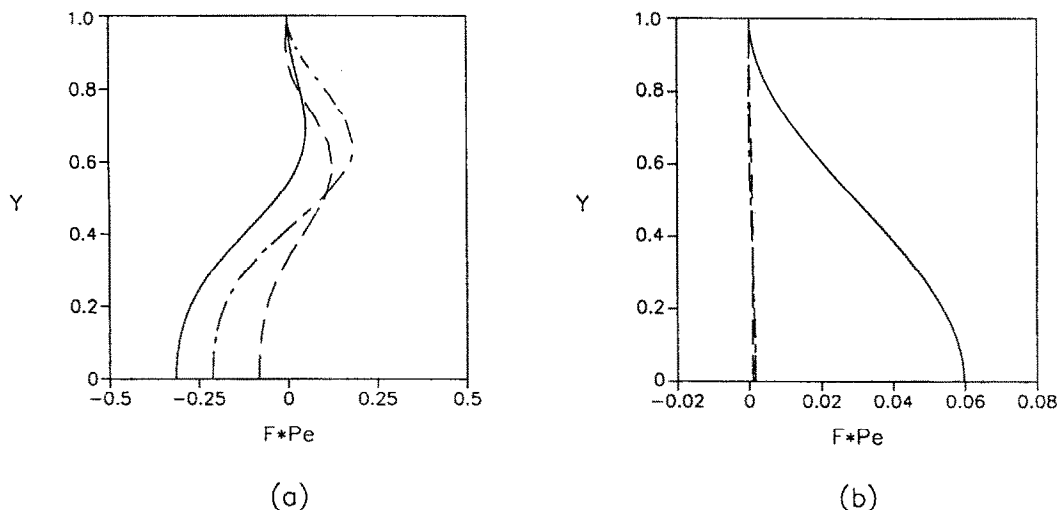
FIG. 9. Plots of F, as shown in equation (8). $A = 0.75$. (a) $X^* = 0.14$, (b) $X^* = 1.85$. ———, $M = 1.0$; ———, $M = 3.0$; ———, $M = 5.0$.

changes in heat transports are caused predominantly by the axially advective term, i.e.

$$F \equiv \left[\frac{\partial}{\partial X} (u_t \theta_t) \right]_m - \frac{\partial}{\partial X} (u_s \theta_s), \qquad (8)$$

in which subscripts t and s refer, respectively, to pulsating and non-pulsating flow, and m indicates time-averaging over a cycle. This observation is supportive of the earlier conclusion by Faghri et al. [12], although the linearized analysis by [12] was directed to more restricted flow regimes and in rather limited scopes of parameters.

The above-derived F is a function of the spatial position and of M. The exemplary structure of F is illustrated in Fig. 9. Clearly, the overall magnitudes of F are appreciable in the upstream regions close to the entrance, but they diminish in the downstream regions, say $X^* > 1.0$ for the case of the parameter set of Fig. 9 (note the difference in scales for the abscissa in Fig. 9). It is also apparent that, in the moderate and far downstream regions, F is practically zero when the frequency parameter is large. The behavior of the y-integrated value of $F \cdot Pe$ is consistent with that of $(Nu_{t-s})_m$ depicted in Figs. 5–7.

Further physical insight is gained by decomposing this additional axial convection effect F. Note that F can be rewritten as

$$F \equiv u_s \left(\frac{\partial \theta'}{\partial X} \right)_m + (u')_m \frac{\partial \theta_s}{\partial X} + \left(u' \frac{\partial \theta'}{\partial X} \right)_m \qquad (9)$$

where subscript s refers to the steady non-pulsating part, and prime denotes the time-dependent fluctuation.

The time-dependent fluctuation of the axial temperature gradient is Fourier-series represented

$$\frac{\partial \theta'}{\partial X} (X, Y, \tau) \equiv G_0 + \sum_{n=1}^{\infty} G_n \cdot \sin (n\omega\tau + \phi_n). \qquad (10)$$

In the above, G_0 indicates the constant part, i.e. the rectification of a time-dependent function, and ϕ_n reflects the phase difference of the nth component relative to the inlet velocity. Similarly, the time-dependent velocity fluctuation in the fully developed region is expressed as

$$u'(Y, \tau) \equiv \sum_{n=1}^{\infty} U_n \cdot \sin (n\omega\tau). \qquad (11)$$

The typical structure of $\partial \theta'/\partial X$ is plotted in Fig. 10. Obviously, in the upstream region close to the entrance, the overall magnitudes of $\partial \theta'/\partial X$ are substantial, especially for low values of M (see Fig. 10(a)). However, $\partial \theta'/\partial X$ weakens in the downstream regions (see Fig. 10(b); note the difference in scales for the ordinates in Figs. 10(a) and (b)). It is readily recognized in Fig. 10(a) that both the rectification, i.e. the magnitude of the average value, G_0, and the presence of the higher harmonics in equation (9) are significant. This leads to the interpretation that, in the upstream region close to the entrance, the impact of the higher harmonics is noticeable in the thermal field.

As reported by the preceding accounts on pulsating flow field characteristics [1, 2, 11, 14], u' in equation (11) is predominantly made up of the base harmonic of the forced pulsating frequency, U_1, and the magnitudes of the higher harmonics are negligibly small. Consequently, the major contributor to F in equation (9) turns out to be the third term on the right-hand side, $(u' (\partial \theta'/\partial X))_m$. This term represents the interaction of the velocity and temperature oscillations, and this effect was described as an extra diffusivity by Faghri et al. [12]. When the prior relations are substituted, they yield

$$\left(u' \frac{\partial \theta'}{\partial X} \right)_m = \frac{U_1 \cdot G_1}{2} \cos (\phi_1), \qquad (12)$$

and, therefore,
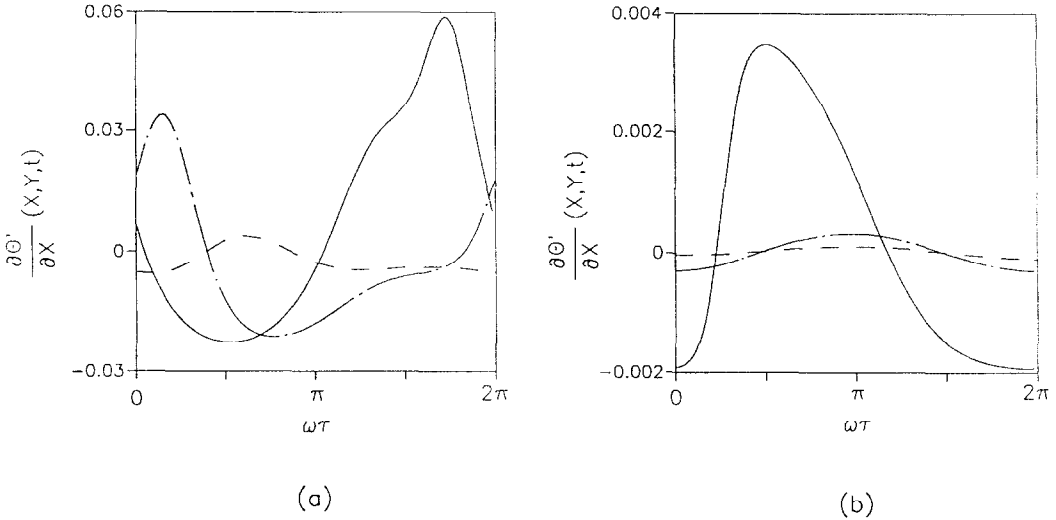
FIG. 10. Time variations of the fluctuating part of the axial temperature gradient. $A = 0.75$. Locations are
(a) $[X^*, Y] = [0.14, 0.0]$, (b) $[X^*, Y] = [1.85, 0.0]$. ——, $M = 1.0$; ———, $M = 3.0$; ----, $M = 5.0$.

$$F = u_s \cdot G_o + \frac{U_1 \cdot G_1}{2} \cos(\phi_1). \qquad (13)$$

It is interesting to note that the crucial part of $(\partial \theta' / \partial X)$ is the base harmonic G_1, which is in tune with the forcing pulsation frequency of the inlet velocity. The phase advance ϕ_1 of the G_1-component, relative to the inlet velocity, determines whether the overall heat transfer is enhanced or reduced at that particular location.

The preceding illustrations of the numerical results were given for $Re = 50$. However, additional calculations were conducted for other values of Re. The results of these computations were qualitatively the same as those for $Re = 50$. These point to the observation that the data displayed in Figs. 2–8 are representative of heat transfer characteristics of slow pulsating flows.

The overall heat transport process may be described in general physical terms. For a non-pulsating flow in a channel of constant wall temperature $(T_w > T_o)$, the bulk temperature of fluid will develop a positive axial gradient. This bulk temperature gradient is high in the entrance regions, and it diminishes as the axial location moves downstream. Therefore, at some far downstream axial positions, the bulk temperature approaches T_w and, thereafter, the axial gradient of fluid temperature becomes negligibly small.

As succinctly expounded by previous studies [12, 17–21], the net effect of flow oscillation gives rise to substantial extra diffusivity. This has been well established, e.g. by Watson [19] and Joshi *et al.* [20], and only the highlights of this concept are briefly recapitulated here for definiteness. The velocity and temperature can be divided into two components, i.e. one representing the mean value and the other denoting deviation from this mean value;

$$u(x, y, t) = \bar{u}(x) + u'(x, y, t)$$

$$T(x, y, t) = \bar{T}(x) + T'(x, y, t). \qquad (14)$$

In the above, a barred quantity is defined as

$$\bar{\phi} \equiv \frac{1}{A_h P} \int_0^{A_h} \int_0^P \phi \, dt \, dA_h$$

where P is the oscillation period and A_h the channel cross-sectional area. Accordingly, the instantaneous heat flux in the axial direction may be written as

$$q_x = uT - \alpha \frac{\partial T}{\partial x}. \qquad (15)$$

Upon substituting equation (14) into equation (15), and taking the mean value yields

$$\bar{q}_x = \bar{u}_s \bar{T}_s + \bar{u}_s \bar{T}_{1-s} + \overline{u'T'} - \alpha \frac{\partial \bar{T}}{\partial x}, \qquad (16)$$

which can be rewritten as

$$\bar{q}_x = \bar{u}_s \bar{T}_s - K \frac{d\bar{T}}{dx}. \qquad (17)$$

where $K/\alpha \equiv 1 - (\bar{u}_s \bar{T}_{1-s} + \overline{u'T'})/(\alpha \cdot d\bar{T}/dx)$.

Equation (17) is similar to the expression obtained previously by Joshi *et al.* [20]. This clearly indicates that there exist heat transport in the axial direction by the oscillation-induced effective diffusivity K. References [17–21] demonstrated that K/α is always positive and larger than unity. In fact, K/α is usually much larger than one, which implies an effective amplification of conductive heat transfer by oscillation. Figure 11 displays an exemplary plot of K/α.

The physical explanation for the behavior of heat transfer between the fluid and the wall may now be better understood. In the entrance region, the axial bulk temperature gradient is steep, and the fluid temperature is raised, in comparison to the case of a non-pulsating flow, as a result of this heat transfer in the
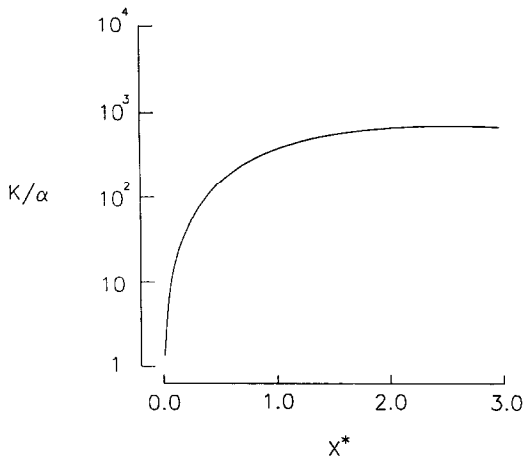
FIG. 11. Axial variations of the effective thermal diffusivity K. $M = 1.0$, $A = 0.75$.

FIG. 12. Axial profiles of the bulk temperature of a pulsating and a non-pulsating flow. $A = 0.75$. ——, $M = 1.0$; ---, $M = 2.0$.

negative X-direction. The heat transfer rate from the channel wall of T_w to the fluid is thus reduced from that of a non-pulsating flow. This process is shown up in zone (I) of Fig. 8. At moderate downstream locations, the axial gradient of bulk temperature becomes, in general, less steep as the axial location moves downstream. The heat transports by the oscillation-induced extra diffusivity will vary along the axial location accordingly. The oscillation-induced heat conduction is more effective near the entrance region than near the far-downstream region. The net result is that the bulk temperature at moderate downstream locations, therefore, tends to be lower than that of a non-pulsating counterpart. This leads to the conclusion that the heat transfer from the channel wall to the fluid is increased for a pulsating fluid, and this turns up as zone (II) in Fig. 8. At far downstream locations, the fluid bulk temperatures are essentially T_w, and the oscillation-induced diffusivities are ineffective in rendering any changes in overall heat transport process. This is indicated in zone (III) of Fig. 8. In order to provide further credence to the above physical argument, the axial profiles of the bulk temperatures of a pulsating flow and of a corresponding non-pulsating flow are plotted in Fig. 12. The axial behavior of these temperature profiles is consistent with the physical reasoning given in the above.

Taking advantage of the wealth of comprehensive numerical data, validation was made of the correctness of the above procedures. On one hand, the values of F secured by direct numerical computations in equation (8), as displayed in Fig. 9, were digitized. On the other hand, the computed results of u' and $\partial\theta'/\partial X$ were decomposed respectively into the Fourier series. The calculated values of U_1, G_1 and ϕ_1 were utilized to yield $(u'(\partial\theta'/\partial X))_m$ as in equation (12). These two sets of the values were found to be in close agreement.

The present numerical studies shed some light on
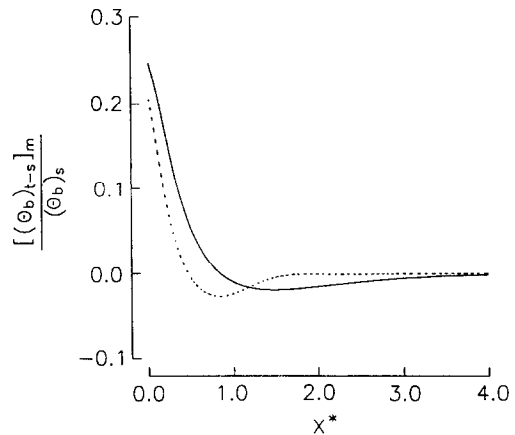
the long-standing discrepancies that have been reported on heat transfer properties of a pulsating flow. As stated previously, some previous investigations showed heat transfer augmentations, while others claimed heat transfer reductions or no changes. These apparently reflect the fact that some of these preceding studies were performed in a piecemeal fashion in the parameter space as well as in choosing the location of the channel. As displayed in the present endeavor, both local heat transfer enhancement and decrease can be expected in various axial locations of the channel, and these results depend on other relevant parameters in a rather complicated manner.

4. CONCLUSION

The afore-mentioned results of the numerical exercise point to the following observations. The flow field data are in broad agreement with the preceding analytical findings. When M is low, the velocity profiles resemble much of the quasi-steady solutions. When M is large, the effects of oscillation are confined to a narrow zone adjacent to the walls.

The effects of pulsation on Nu are pronounced for large A and in the upstream entrance regions, say $X/(Re \cdot Pr) < 1.0$. Changes in Nu due to pulsation are appreciable throughout much of the channel length when M is low and moderate. At high pulsation frequencies, $M > 1.0$, changes in Nu are generally minor. In comparison to the case of a non-pulsating flow, reduction in local Nu is expected at low pulsation frequencies and in the extreme upstream region, and enhancement in local Nu is anticipated at moderate downstream locations. At locations further downstream, Nu remains virtually unchanged.

Detailed analyses on local behavior of Nu were performed by representing the numerically-obtained flow data in the Fourier series. In consistency with the preceding theoretical endeavors [12], the dominant contributor to the change in Nu stems from the

additional axial transport effect F. It is shown that the extra diffusivity term plays the most significant role. This overall effect can be demonstrated to depend crucially on the pulsating velocity component U_1, and the basic harmonic G_1 of $\partial\theta'/\partial X$, and the phase advance ϕ_1 of G_1 relative to the inlet velocity.

REFERENCES

1. S. Uchida, The pulsating viscous flow superposed on the steady laminar motion of incompressible fluid in a circular pipe, *ZAMP* **7**, 403–422 (1956).
2. H. B. Atabek and C. C. Chang, Oscillatory flow near the entry of circular tube, *ZAMP* **12**, 185–201 (1961).
3. H. B. Atabek, C. C. Chang and L. M. Fingerson, Measurement of laminar oscillatory flow in the inlet length of a circular tube, *Phys. Med. Biol.* **9**, 219–227 (1964).
4. P. J. Florio and W. K. Mueller, Development of a periodic flow in a rigid tube, *Trans. ASME J. Basic Engng* **90**(3), 395–399 (1968).
5. E. B. Denison, W. H. Stevenson and R. W. Fox, Pulsating laminar flow measurements with a directionally sensitive laser velocimeter, *A.I.Ch.E. Jl* **17**(4), 781–787 (1971).
6. J. H. Gerrard and M. D. Hughes, The flow due to an oscillating piston in a cylindrical tube: a comparison between experiment and a simple entrance flow theory, *J. Fluid Mech.* **50**(1), 97–106 (1971).
7. M. Clamen and P. Minton, An experimental investigation of flow in an oscillating pipe, *J. Fluid Mech.* **81**, 421–431 (1977).
8. D. M. Eckmann and J. B. Grotberg, Experiments on transition to turbulence in oscillatory pipe flow, *J. Fluid Mech.* **222**, 329–350 (1991).
9. M. F. Hwang and A. Dybbs, Heat transfer in a tube with oscillatory flow, ASME Paper 83-WA/HT-90, 1–12 (1983).
10. T. W. Simon and J. R. Seume, A survey of oscillating flow in Stirling engine heat exchangers, NASA Contractor Report 182108 (1988).
11. R. Siegel and M. Perlmutter, Heat transfer for pulsating laminar duct flow, *Trans. ASME J. Heat Transfer* **84**(2), 111–123 (1962).
12. M. Faghri, K. Javdini and A. Faghri, Heat transfer with laminar pulsating flow in a pipe, *Lett. Heat Mass Transfer* **6**, 259–270 (1979).
13. R. Siegel, Influence of oscillation-induced diffusion on heat transfer in a uniformly heated channel, *Trans. ASME J. Heat Transfer* **109**, 244–247 (1987).
14. H. W. Cho and J. M. Hyun, Numerical solutions of pulsating flow and heat transfer characteristics in a pipe, *Int. J. Heat Fluid Flow* **11**(4), 321–330 (1990).
15. D. O. Barnett and R. I. Vachon, An analysis of convective heat transfer for pulsating flow in a pipe, *Proc. 4th Int. Heat Transfer Conference*, Paris, pp. 1–11 (1970).
16. S. V. Patankar, *Numerical Heat Transfer and Fluid Flow*. Hemisphere, Washington, D.C. (1980).
17. P. C. Chatwin, On the longitudinal dispersion of passive contaminant in oscillatory flows in tubes, *J. Fluid Mech.* **71**, 513–527 (1975).
18. R. Smith, Contaminant dispersion in oscillatory flows, *J. Fluid Mech.* **114**, 379–398 (1982).
19. E. J. Watson, Diffusion in oscillatory pipe flows, *J. Fluid Mech.* **133**, 233–244 (1983).
20. C. H. Joshi, R. D. Kamm, J. M. Drazen and A. S. Slutsky, An experimental study of gas exchange in lamina oscillatory flow, *J. Fluid Mech.* **133**, 245–254 (1983).
21. U. H. Kurzweg, Enhanced heat conduction in oscillating viscous flows within parallel-plate channels, *J. Fluid Mech.* **156**, 291–300 (1985).